Comparison of Redundancy Requirements for Modular Multilevel Converter Considering Manufacturer Reliability Inputs and Mission Profile

Diego Velazco[1,2], Guy Clerc[1,2], Emmanuel Boutleux[1,2], François Wallart[1]

[1] SUPERGRID INSTITUTE SAS
23 rue Cyprian
Villeurbanne, France
Tel.: +33 / (0) – 4 28 01 23 23
E-Mail: Diego.VELAZCO@supergrid-institute.com
URL: https://www.supergrid-institute.com/

[2] Univ. Lyon, Univ. Claude Bernard Lyon1, INSA Lyon, Ecole Centrale Lyon, AMPERE UMR CNRS 5005

Acknowledgements

This work was supported by a grant overseen by the French National Research Agency (ANR) as part of the "Investissements d'Avenir" Program (ANE-ITE-002-01).

Keywords

«Modular Multilevel converters (MMC)», «HVDC», «Mission profile», «Lifetime», «Reliability».

Abstract

During the design phase, target reliability values of components – including semi-conductors - allow the computation of converter level reliability and redundancy requirements. This work proposes a more accurate method based on manufacturer lifetime models and mission profile evaluation. The new method is applied on a Modular Multilevel Converter.

I - Introduction

The growing needs of power transmission systems are pushing towards the rapid development of HVDC technologies. Moreover, HVDC has been recognized as a major contender for performing long-distance bulk-power transmission [1], [2]. Among HVDC technologies, voltage source converters (VSC-HVDC) are considered the most suitable to interact with existing AC grids [3]. Nowadays, the most promising VSC-HVDC topology is the Modular Multilevel Converter (MMC) [4], [5].

The MMC for HVDC applications is a three-phase converter as seen in Fig. 1 (a). Each phase comprises an upper and a lower arm. Each arm is composed of a stack of submodules (SMs) and an arm inductor. The SMs are connected in series in order to withstand the high voltage levels inherent to HVDC systems. Multiple SM configurations are proposed in the literature, but the two most popular are the half-bridge (HB-SM) and the full-bridge (FB-SM) configurations. Today, in practical applications, the HB-SM is the most used due to cost considerations. To guarantee the proper functioning of the converter, a large number of SMs must be installed in each arm. In the case of HVDC applications the number of HB-SMs is in the range of some hundreds per arm.

A HB-SM consists of a storage capacitor C, two IGBT T1 and T2 and two antiparallel connected diodes D1 and D2 as depicted in Fig. 1 (b). The different semiconductors allow the insertion, or the bypass of the capacitor and they will be active based on the command signals and the direction of the current.

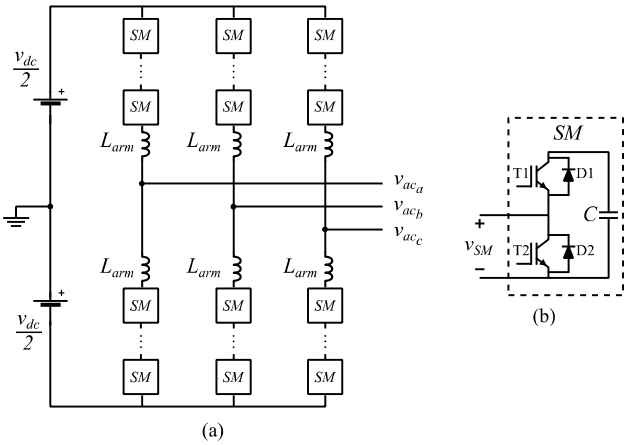

Fig. 1: (a) MMC topology, (b) Half-bridge submodule

Given the criticality of energy outages and its potential repercussions, special care should be taken for assessing the reliability of HVDC technologies such as the MMC. According to the ENTSOE, improved reliability (e.g. decreasing 1-2 trips per year) and improved availability (e.g. decreasing 1-2 outages days per year) can bring significant cost savings to TSOs and / or society [6].

Having such demanding reliability constraints, MMC arms are equipped with additional SMs for providing the redundancy required for attaining the availability requirements of an HVDC system. This work intends to shed a light on the estimation of the number of redundant SMs. In order to do so, two case studies will be compared: In the first case, the redundancy computation will use out-of-the-shelf reliability indicators from the manufacturer. In the second case, the redundancy will be computed using the mission profile of the converter.

In order to be able to consider the mission profile of the converter and obtain the number of redundant semiconductors, the thermal loading of power devices will be determined thanks to the methodology for lifetime estimation developed in [7].

This work will present the profile-based lifetime estimation methodology in Section II. Then Section III will depict the methodology for performing reliability predictions of the different elements of a SM. Section IV presents the methodology for translating the reliability calculations of a SM into redundancy requirements. Section V discusses the reliability predictions and redundancy estimations and gives a comparison on the two case studies. Finally, section VI gives the conclusions on this research.

II – Methodology for profile-based lifetime estimation

The methodology employed for considering the mission profile for the lifetime estimation of the power semiconductors [7] can be summarized in Fig. 2. It consists of 5 different stages: the modeling of the converter, the calculation of the losses of the semiconductor devices, the calculation of the thermal loading, the use of the rain flow counting algorithm [8] for organizing the thermal profiles and finally, the use of the lifetime models provided by the manufacturer as well as the Miners rule [9] for estimating the lifetime consumption.

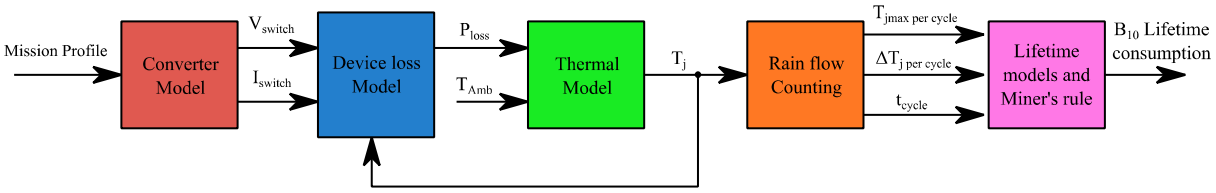

Fig. 2: Flowchart of the lifetime estimation methodology

An important step in the lifetime estimation methodology is the assessment of the temperature profile of the different semiconductors. This stage is performed considering two different timescales as seen in

[7]. The thermal profiles obtained for the studied mission profile, which corresponds to an offshore wind farm (OWF), can be seen in Fig. 3. Then the thermal profiles are organized thanks to the rain flow counting algorithm as seen in the left portion of Fig. 4.

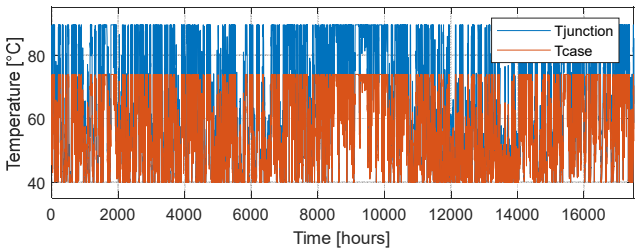

Fig. 3: Thermal profile of T2 under the evaluated period for the studied mission profile

One of the hallmarks presented in this methodology is the introduction of the model-based extrapolation method [7] for obtaining the B10 number of cycles to failure. The extrapolation method is necessary to be able to use the manufacturer lifetime models [10] for estimating the lifetime consumption in the evaluated period. The extrapolation method is constructed thanks to the Norris-Landzberg lifetime model [11], yielded by expression (1) and which results in the extrapolation grid shown in the central portion of Fig. 4.

$$N_{f1} = N_{f2}\left(\frac{\Delta T_2}{\Delta T_1}\right)^{\alpha}\left(\frac{t_2}{t_1}\right)^{\beta} exp\left(\gamma\left(\frac{1}{T_1}-\frac{1}{T_2}\right)\right) \quad (1)$$

In (1), Nf_1 represents the number of cycles to failure for condition 1 (resp. for Nf_2), ΔT_1 the temperature swing for condition 1 (resp. for ΔT_2), t_1 the cycle duration for condition 1 (resp. for t_2) and T_1 the temperature reference for condition 1 (resp. for T_2). Coefficients α, β and γ can vary according to the evaluated conditions. The grid shown in the central portion of Fig. 4 allows for the calculation of the new coefficients α, β and γ for each cycling condition. These coefficients are computed for each mesh with least-squares algorithm considering the vertices of the mesh.

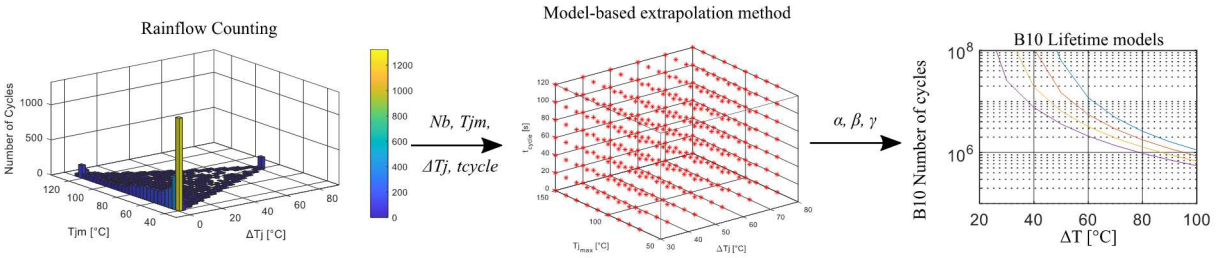

Fig. 4: Grid for model-based extrapolation method

The manufacturer provides different curves for performing the lifetime estimation of the different elements of the semiconductor devices such as the chip solder, the baseplate solder, and the bond wires [10]. The yearly B10 lifetime consumption, $CL_{i,k}$ for the k^{th} element (chip solder, dbc solder or bondwire) and i^{th} thermal cycle identified is obtained with (2). In (2), nb_i is the number of cycles for a given thermal condition and $Nf_{i,k}$ is the number of cycles to failure for the same condition. Moreover, the expected time LF_k for a 10% failure rate of the k^{th} element of the semiconductors can be calculated with (3). In (3), N_{cyc} is the total number of thermal cycles in the evaluated period. Some of the lifetime consumption results for the evaluated profile can be seen in Fig. 5.

$$CL_{i,k} = \frac{nb_i}{N_{fi,k}}, k \in \{\text{chip solder, dbc solder, bondwire}\} \quad (2)$$

$$LF_k = \frac{1}{\sum_{i=1}^{N_{cyc}} CL_{i,k}}, k \in \{\text{chip solder, dbc solder, bondwire}\} \quad (3)$$

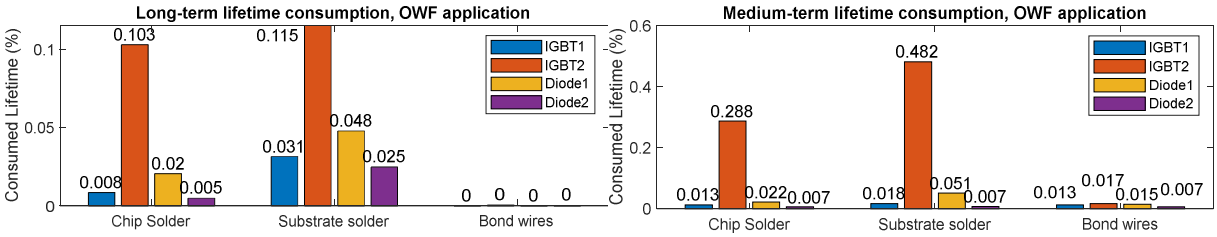

Fig. 5: Lifetime consumption results (a) Long-term timescale (b) Medium-term timescale

III – Methodology for reliability predictions

In this work the reliability predictions are performed considering two different case studies: manufacturer off-the-shelf reliability indicators and mission profile-based reliability estimations.

For the first case, the inputs considered are the failure rates of the different elements that compose a SM, such as the power semiconductors, the storage capacitor and the electronic board that drives the SM as done in [12]. The failure rates of these components, expressed in FIT are depicted in Table I.

Table I: FIT values for the SM elements [12]

Component	FIT
IGBT	100
Capacitor	300
Control Board	1200

Having the failure rates λ, of the elements of a SM the calculation of the failure rate of a SM λ_{SM}, can be calculated with (4) by adding the failure rates of the different elements of the SM and subsequently the reliability of a SM $R_{SM}(t)$ can be computed employing (5).

$$\lambda_{SM} = 2 \cdot \lambda_{IGBT} + \lambda_{capacitor} + \lambda_{board} \tag{4}$$

$$R_{SM}(t) = e^{-(\lambda_{SM} \cdot t)} \tag{5}$$

It is also worth mentioning that for the case in which only off-the-shelf reliability indicators are employed, the reliability function is obtained employing an exponential distribution. This method does not consider wear-out failures. The resulting reliability distribution for this case can be seen in Fig. 6.

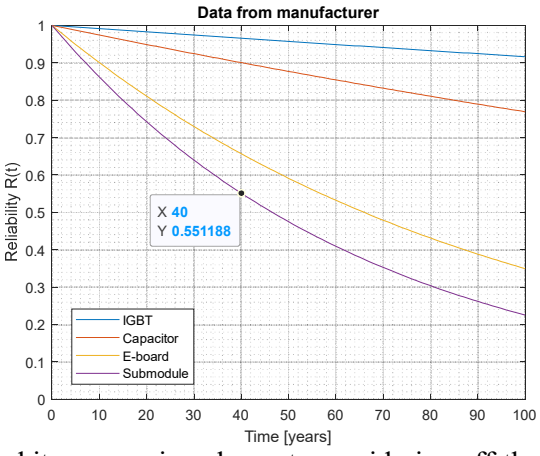

Fig. 6: Reliability of a SM and its composing elements considering off-the-shelf reliability indicators

The second case considers the mission profile experienced by the converter and employs the results obtained in section II as inputs. The profile evaluated in this work corresponds to a 1 GW converter installed in an offshore wind farm. After having calculated the lifetime consumptions of the elements of the semiconductors in the evaluated period and under the evaluated profile, the lifetime for a 10% failure

rate is calculated by using the data from [10]. This result can be translated into a device level reliability function as depicted in Fig. 7.

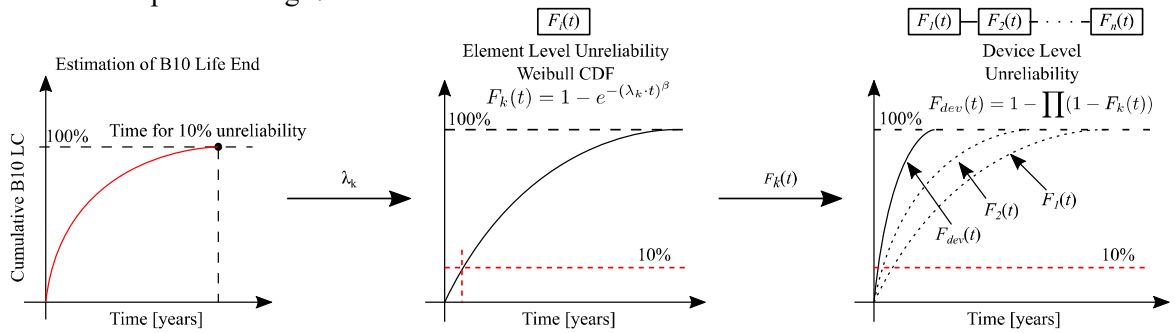

Fig. 7: Methodology for calculating device level reliability indicators

As the manufacturer B10 lifetime models [10] are fitted using a two parameter Weibull distribution (6), (7) will allow the calculation of the failure rate describing the cumulative density function CDF, for the elements of the semiconductors. In (7), the CDF $F_k(LF_k) = 0.1$. It is worth noting that different shape factors β were evaluated for the semiconductor devices in this study, as this parameter represents the variance of the instantaneous failure distribution of the studied elements. Having calculated the individual CDF for the elements of the semiconductors, the unreliability for the semiconductor devices $F_{dev}(t)$ can be obtained with (8).

$$F_k(t) = 1 - e^{-(\lambda_k \cdot t)^\beta}, k \in \{\text{chip solder, dbc solder, bondwire}\} \quad (6)$$

$$\lambda_k = -\frac{[ln(1-F_k(LF_k))]^{1/\beta}}{LF_k}, k \in \{\text{chip solder, dbc solder, bondwire}\} \quad (7)$$

$$F_{dev}(t) = 1 - \prod\big(1 - F_k(t)\big), dev \in \{T1, D1, T2, D2\} \quad (8)$$

Once the unreliability function of all the semiconductors is obtained, the unreliability of the SM can be obtained with (9). In (9), m represents all the different elements of the SM such as the semiconductor devices T1, D1, T2 and D2, as well as the capacitor and electronic board. The failure distribution of the capacitor and the electronic board are calculated with an exponential distribution, as done in the previous case study (off-the-shelf reliability indicator). With the failure distribution of a SM, its reliability function can be deduced with (10). Fig. 8 depicts the reliability functions of the elements of a SM. The results in Fig. 8 were obtained with β = 2.5.

$$F_{SM}(t) = 1 - \prod\big(1 - F_m(t)\big), m \in \{T1, D1, T2, D2, Capacitor, Board\} \quad (9)$$

$$R_{SM}(t) = 1 - F_{SM}(t) \quad (10)$$

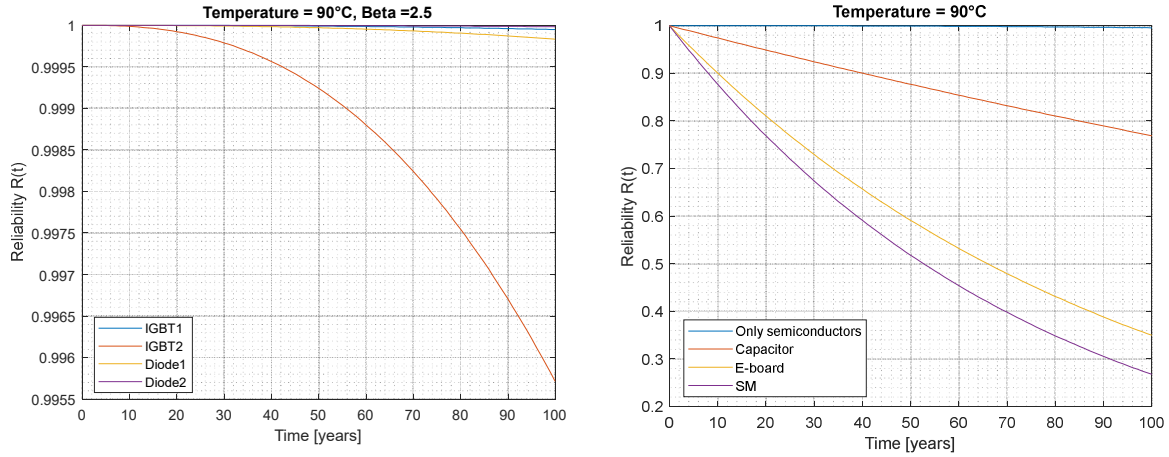

Fig. 8: Reliability of a SM and its composing elements considering the mission profile (β=2.5)

In Fig. 9, the resulting reliability functions of the SMs for the two case studies can be appreciated. The profile-based case study considered different shape factors β for the reliability computations. The values considered are 1, 1.5, 2, 2.5, 5 and 10 as depicted in Fig. 9.

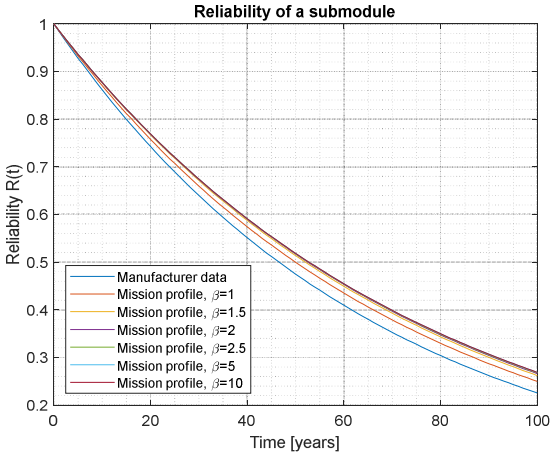

Fig. 9: Reliability functions of a SM for the studied cases

It can be seen from Fig. 9, that manufacturer off-the-shelf data yields the more pessimistic reliability prediction when compared to the profile-based reliability estimation. The results considering the mission profile are notably dependent on the thermal conditions chosen for the study. The lifetime models employed depend greatly on the thermal profile experienced by the semiconductors and more particularly on the variation of the experienced thermal cycles ΔT.

For the purpose of this study and in order to obtain realistic results, a maximum junction temperature of 90°C was considered for the semiconductor devices as seen on Fig. 3. This requirement was then used for dimensioning the thermal characteristics of the heatsink associated to the semiconductors. If a higher maximum junction temperature would have been considered, the profile-based reliability calculations would yield significantly lower and worse results.

Additionally, it can be said from Fig. 9 that, given the thermal constraint imposed to the semiconductors, the shape factor β in the range [1.5 10] doesn't have a great influence on the final reliability computation of the SM. Moreover, since the reliability function for the capacitor and the control board are the same in all the configurations, the final SM reliability estimation is mostly dependent on those elements, as they have considerably higher failure rates than the semiconductors.

IV – Methodology for redundancy estimations

Knowing the reliability distribution of a SM allows the calculation of the reliability function of an MMC arm. In order to make a realistic evaluation of the arm reliability a Markov chain was developed for this purpose as depicted in Fig. 10. Along with the Markov chain, Monte Carlo simulations were performed for assessing multiple converter lifetimes. For the purpose of the simulations a target mission time of 40 years was considered.

Consequently, different redundancy levels were tested. For each redundancy level, 1000 simulations were carried out. The minimum number of SMs to be installed in an arm should guarantee a reliability of 99.5 % by the end of the target mission time of the converter. Maintenance is also considered for the simulations. At each maintenance period, if the number of failed SMs is smaller than the number of redundant SMs, all the failed ones are replaced. However, if at any point throughout the simulations the amount of failed SMs is bigger than the number of redundant SMs, then the converter has failed that test. A maintenance intervention every two years was considered for the Monte Carlo simulations. The arm reliability is approximated to the number of arm survivals for a given redundancy level.

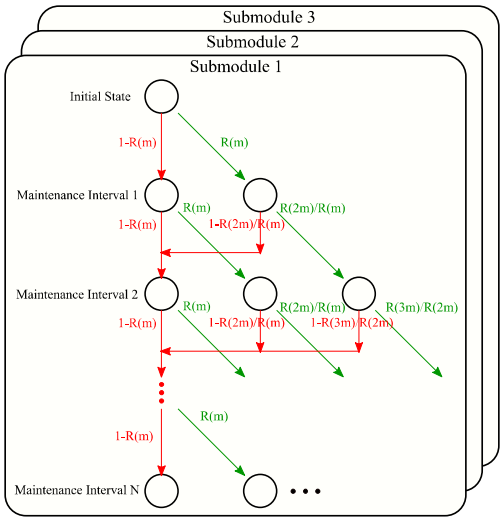

Fig. 10: Markov chain for calculating the availability of the converter for a target mission time

This methodology allowed for the calculation of the redundancy requirements of the MMC for the two case studies. These results can be seen in Fig. 11.

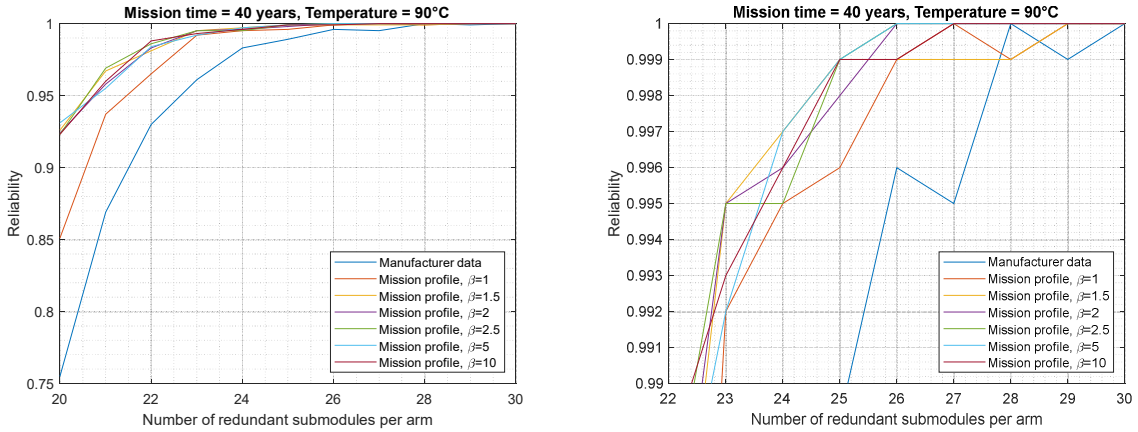

Fig. 11: Reliability of an MMC arm vs number of redundant SMs

As mentioned previously in this section, the chosen criteria for determining the number of redundant SMs required for an MMC arm is to guarantee a reliability of 99.5% throughout its operating life. Thus, the number of redundant SMs required for each of the evaluated cases can be seen in Table II.

Table II: Number of redundant SMs for a 40-year target mission time and 99.5% reliability

Case Study	Manufac-turer data	Mission profile, β=1	Mission profile, β=1.5	Mission profile, β=2	Mission profile, β=2.5	Mission profile, β=5	Mission profile, β=10
Redundant SMs	26	24	23	24	23	24	24

V – Discussion on the results of the reliability predictions and redundancy estimations

The number of redundant SMs reflects the reliability functions calculated in section III. The results depicted in Table II and Fig. 11 indicate that using the manufacturer reliability indicators yields the worst-case scenario for redundancy dimensioning. As mentioned in section III, the thermal constraints imposed to the converter have a significant impact on the redundancy requirements obtained in the profile-based redundancy calculations.

The results seen in Table II show that the shape factor β used for calculating the reliability distributions of the semiconductors has almost no impact on the final redundancy estimations. This is mainly due to the fact that the failure rates of the storage capacitor and the control board of the SM are much higher than the failure rates of the semiconductors in both case studies.

In a Weibull distribution, the shape factor β allows the modeling of the wear-out of the studied element when β>1. The reason why there is not a noticeable loss of reliability in spite of the different β evaluated, is that the acceleration in the reliability decline happens much after the target mission time of the converter. An example concerning the reliability of the chip solder of IGBT 2 can be seen in Fig. 12.

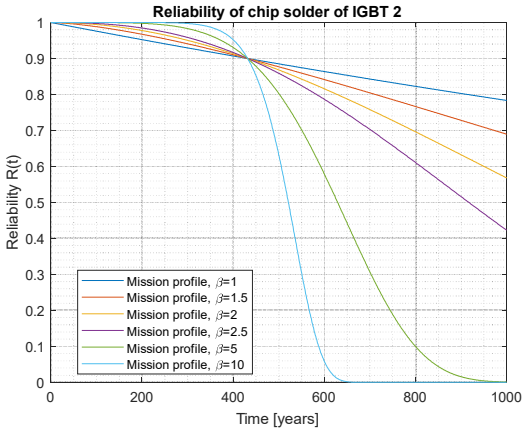

Fig. 12: Reliability of chip solder of IGBT 2 for different β

The reliability functions seen on Fig. 12 are obtained considering a fixed time span for a loss of reliability of 10%, which corresponds to the B10 definition in [10]. The fixed time span for the loss of reliability is the result of (3) in the lifetime estimation methodology described in section II.

Another noticeable result from this research is the estimation of the number of failed SMs at each maintenance period. This result allows the calculation of the approximated amount of SMs required for a proper functioning of an MMC arm throughout all the target mission time of the converter (40 years). These calculations were possible thanks to the Monte Carlo simulations and the Markov chain depicted in Fig. 10. In Fig. 13(a), the number of failed SMs for the profile-based redundancy calculations can be seen. The results correspond to a shape factor β = 2.5. Consequently, in Fig. 13(b), the number of SMs employed during the operating life of the converter arm can be seen.

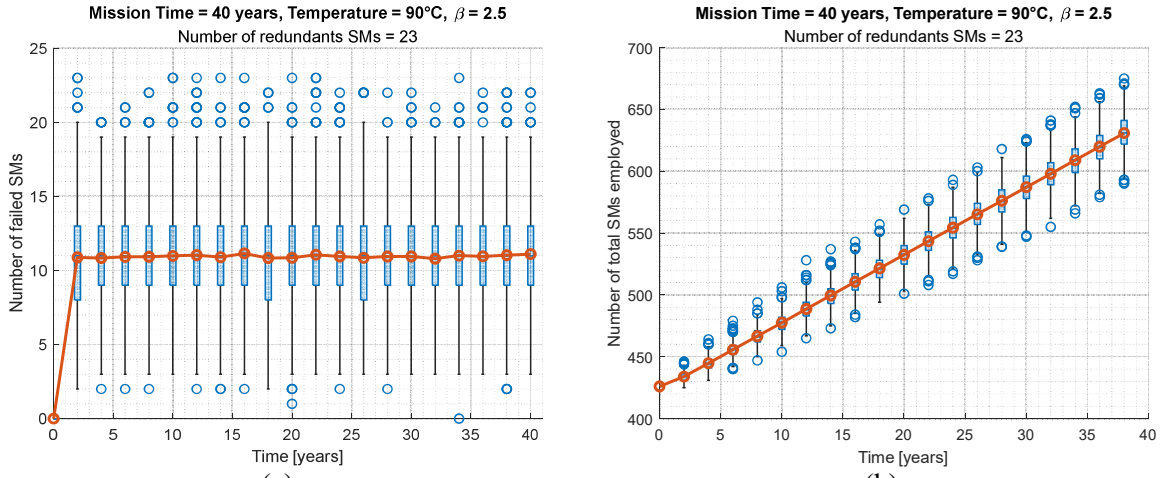

(a) (b)

Fig. 13: (a) Number of failed SMs per arm at each maintenance intervention (1000 Monte Carlo tests), (b) Number of total SMs employed during the operating life of the converter arm

In Fig. 13(a), it can be seen that the maximum number of failed SMs at a given maintenance intervention is equal to the number of redundant SMs installed. If the number of failed SMs would have been higher, the MMC arm wouldn't have survived and the whole converter would have stopped working. The average number of failed SMs per maintenance period is 11, but it can have a large variance as evidenced on Fig. 13(a).

It can be seen from Fig. 13(b), that the total number of SMs employed throughout the operating life of the converter is indeed much higher than the minimum number of SMs required for the arm functioning. The studied MMC arm requires only 400 SMs to operate, it requires 23 redundant SMs to guarantee a reliability of at least 99.5% by the end of its target mission time and in total, it will require 631 SMs in average. This means that the converter arm requires more than 200 additional SMs than the ones with which it started working, which by no means is a negligeable amount and can have a great impact on the OPEX of the converter. Moreover, an MMC has six arms, so the total number of SMs employed in the whole converter throughout its target mission time can ascend to 3800 SMs in average, a very large amount when compared to the 2400 SMs, required for MMC operation. A comparison between the total number of SMs employed for all the cases can be seen in Fig. 14.

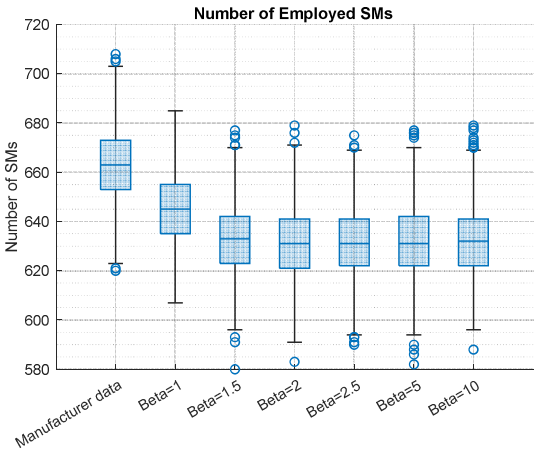

Fig. 14: Comparison between the number of employed SMs

As mentioned previously, the shape factor β employed for the profile-based redundancy calculations does not affect notably the number of redundant SMs (Fig. 11). However, when β=1 a slight impact on the total number of SMs employed can be seen in Fig. 14. The average number of employed SMs when β=1 is 645, compared to 631 for the other profile-based redundancy estimations where β>1. It is worth reminding that when β=1, the Weibull distribution behaves as an exponential distribution. As it was shown in Fig. 12, with β>1 an acceleration in the decline of the reliability distribution is expected. However, this decline happens much after the target mission time of the converter, that means that before this decline the reliability distributions that have a higher shape factor β will have higher reliability values, as it was seen in Fig. 12.

Concerning the total number of the employed SMs that is determined by the manufacturer off-the-shelf reliability indicators, it can be clearly seen in Fig. 14 that this input yields the worse results. The exponential distribution was used to model the reliability function in this case. As previously seen on section III, the reliability function obtained with the manufacturer inputs is the more pessimistic and the number of total employed SMs reflect this condition. The average number of SMs employed with this information ascends to 663, which is bigger than the number of employed SMs coming from the profile-based methodology (645 for β=1 and 631 for β>1).

VI – Conclusion

In this research, the methodology for lifetime estimation and reliability predictions were presented. Additionally, the methodology for performing redundancy computations for an MMC arm was introduced. Two case studies were treated in this paper, one uses off-the-shelf reliability indicators and

the other uses the mission profile experienced by the converter. The profile-based results were strongly influenced by the thermal constraints imposed to the converter.

There is a direct correlation between the reliability function of the SM and the number of redundant SMs to be installed to attain a target reliability by the end of the operating life of the converter. Moreover, this correlation is also reflected on the total number of SMs to be employed throughout the operating life of the converter. It was seen that, in terms of the number of redundant SMs required, the more pessimistic results came from the manufacturer off-the-shelf reliability indicators, whereas the profile-based calculations offered similar results for all the evaluated shape factors β.

When analyzing the total number of SMs employed throughout the operating life of the MMC, the methodology based on manufacturer reliability inputs yielded the poorest results as expected from the reliability predictions. The results obtained with the profile-based methodology show two different behaviors. When $\beta=1$ the number of employed SMs is larger than when $\beta>1$. This is mainly due to the fact that the shape factor influences on the reliability decline after the operating life of the converter.

Finally, it can be said that the study of the number of failed and employed SMs opens up many perspectives for future research. The authors have already started working on some, such as the choice of alternative maintenance strategies concerning the replacement of healthier SMs in order to optimize the number of redundant SMs required or the total number of SMs employed throughout the active life of the MMC.

The methodologies for lifetime estimation and reliability predictions developed in this work, can be generalized to other converter topologies.

References

[1] M. P. Bahrman and B. K. Johnson, "The ABCs of HVDC transmission technologies," *IEEE Power Energy Mag.*, vol. 5, no. 2, pp. 32–44, Mar. 2007, doi: 10.1109/MPAE.2007.329194.

[2] J. D. Páez, D. Frey, J. Maneiro, S. Bacha, and P. Dworakowski, "Overview of DC–DC Converters Dedicated to HVdc Grids," *IEEE Trans. Power Deliv.*, vol. 34, no. 1, pp. 119–128, Feb. 2019, doi: 10.1109/TPWRD.2018.2846408.

[3] J. C. Gonzalez-Torres, J. Mermet-Guyennet, S. Silvani, and A. Benchaib, "Power system stability enhancement via VSC-HVDC control using remote signals: Application on the Nordic 44-bus test system," in *15th IET International Conference on AC and DC Power Transmission (ACDC 2019)*, 2019, pp. 1–6.

[4] R. Marquardt, A. Lesnicar, and J. Hildinger, "Modulares Stromrichterkonzept für Netzkupplungsanwendungen bei hohen Spannungen," *ETG-Conf.*, 2002.

[5] S. Allebrod, R. Hamerski, and R. Marquardt, "New transformerless, scalable Modular Multilevel Converters for HVDC-transmission," in *2008 IEEE Power Electronics Specialists Conference*, Jun. 2008, pp. 174–179. doi: 10.1109/PESC.2008.4591920.

[6] ENTSO-E, "Improving HVDC System Reliability." ENTSO-E, Nov. 2018. [Online]. Available: https://eepublicdownloads.entsoe.eu/clean-documents/Publications/Position%20papers%20and%20reports/entsoe_pp_HVDC_181205_web.pdf

[7] D. Velazco, G. Clerc, E. Boutleux, F. Wallart, and L. Chédot, "IGBT Lifetime Estimation in a Modular Multilevel Converter for bidirectional point-to-point HVDC application," in *2020 22nd European Conference on Power Electronics and Applications (EPE'20 ECCE Europe)*, Sep. 2020, pp. 1–10. doi: 10.23919/EPE20ECCEEurope43536.2020.9215880.

[8] M. Matsuichi and T. Endo, "Fatigue of metals subjected to varying stress," 1968.

[9] Miner, M.A., "Cumulative Damage in Fatigue," *J. Appl. Mech.*, no. 12, pp. A159–A164, 1945.

[10] N. Kaminski, "Load-cycling capability of HiPak IGBT modules. APPLICATION NOTE 5SYA 2043-04." ABB Group, Feb. 04, 2014.

[11] K. C. Norris and A. H. Landzberg, "Reliability of Controlled Collapse Interconnections," *IBM J. Res. Dev.*, vol. 13, no. 3, pp. 266–271, May 1969, doi: 10.1147/rd.133.0266.

[12] J. Wylie, M. C. Merlin, and T. C. Green, "Analysis of the effects from constant random and wear-out failures of sub-modules within a modular multi-level converter with varying maintenance periods," in *2017 19th European Conference on Power Electronics and Applications (EPE'17 ECCE Europe)*, Sep. 2017, p. P.1-P.10. doi: 10.23919/EPE17ECCEEurope.2017.8099246.